A METHOD FOR PREDICTING THE STRESS DISTRIBUTION IN DUCTILE MATRIX COMPOSITE UNDER CYCLIC LOADING

Souta KIMURA*, Jun KOYANAGI, Takayuki HAMA[+] and Hiroyuki KAWADA[++]**
[Souta KIMURA]: imagine-128@fuji.waseda.jp
***Graduate School of Waseda University, ** Institute of Space and Astronautical Science, Japan Aerospace Exploration Agency, [+]Graduate School of Energy Science, Kyoto University, [++]Department of Mechanical and Engineering, Waseda University**

Keywords: *Polymer Matrix Composite, Elasto-plastic Shear-lag Analysis and FEM*

Abstract

A shear-lag model is developed to predict the stress distributions in and around an isolated fibre in single-fibre polymer matrix composite (PMC) subjected to uniaxial tensile loading and unloading along the fibre direction. The matrix is assumed to be an elasto-plastic material that deforms according to J_2 flow theory. The stress distributions are obtained numerically and compared with a different shear-lag model that employs total strain theory as a constitutive equation of the matrix material.

An effect of the difference between the models on the derived stress state is discussed. Axisymmetric FEM is also conducted to validate the stress states obtained from the present analysis. It proves to be in good agreement with the FEM, which illustrates the importance of application of the incremental analysis.

1 Introduction

It is well known that prediction of the mechanical properties of fibre-reinforced plastics (FRP) requires a detailed understanding of the stress states in the constituent materials. Shear-lag models are often used for stress analysis of unidirectional composites with partial damage. Although shear-lag models do not provide detailed information about the spatial variations of stresses within the composite, the stress field obtained from shear-lag analyses is enough for purposes of material failure predictions under monotonic loading.

In many researches, the shear-lag approaches considering plastic deformation of the matrix have been proposed to obtain the stress distributions appropriately [1-3]. Nevertheless, these shear-lag analyses are inadequate to predict the stress states in the case of cyclic loading, since the total strain theory is employed as a constitutive equation of the matrix; the stress distributions are dependent on the strain path [4], and the total strain theory cannot take the variation of the strain path into consideration. Hence, an appropriate prediction of the stress states under cyclic loading requires an application of incremental strain theory [5].

In this paper, we employ an elasto-plastic shear-lag analysis assuming linear strain hardening of the matrix and apply J_2 flow theory as a constitutive equation of the matrix. The crux of the present study is based on combination of the shear-lag analysis and the incremental strain theory. Comparison of the predicted stress distributions with a model using the deformation theory is conducted, and the predicted distributions are also compared with FEM. It was confirmed that in the case of cyclic loading, the present method is valid to predict the stress states appropriately.

2 Elasto-plastic Shear-lag Analysis

2.1 Local Plasticity of Matrix

In SFC (Single Fibre Composite) test, a fibre break is accompanied by the simultaneous formation of a local plasticity or an interfacial debonding. If the fibre-matrix interfacial strength is much higher than the matrix yielding stress, plastic deformation of the matrix can occur instead of initiation of the interfacial debonding as presented in Fig.1. Fig.1 is a typical result for a single fibre break of ECR glass-vinylester composite. Obviously, a group of slip bands in the vicinity of the fibre break is observed in Fig.1. In the present model, we assume that the fibre-matrix interface is so strong that no interfacial

debonding occurs when fibre breaks. The plasticity of the matrix is assumed to be linear strain hardening, and Fig.2 shows a typical stress-strain curve of matrix resin and its elastic-linear strain hardening approximation.

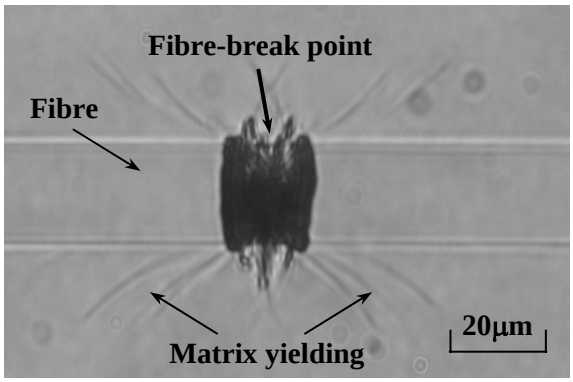

Fig.1. Photograph in the vicinity of a fiber-break point of ECR glass-vinylester composite. A group of slip bands is observed around a fibre break.

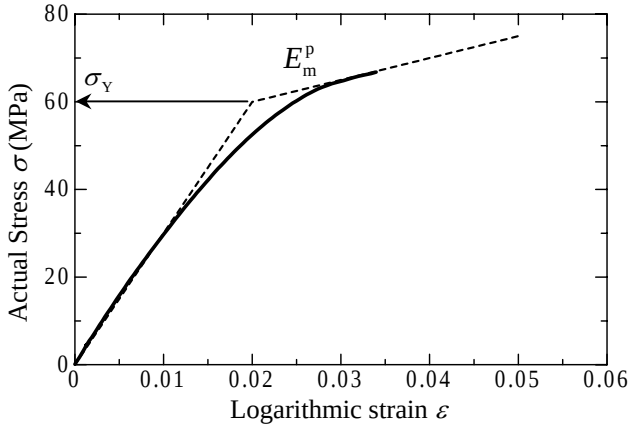

Fig.2. Stress-strain curve of matrix resin (solid line) and elastic-linear strain hardening approximation (dotted line)

2.2 Governing Equation

The model composite of length L consists of a single fibre of radius a encased in a cylindrical matrix of radius b as shown in Fig.3a. As presented in Fig.3b, we divide the matrix into tensile matrix and interfacial layer. The tensile matrix is assumed to be loaded in pure axial stress. In the interfacial layer, the normal stress in the z-direction is not sustained and the shear strain in the radial direction is assumed to be constant. Moreover, we choose the thickness of the interfacial layer, h, as $2a$ from an energy interpretation described in Appendix A.

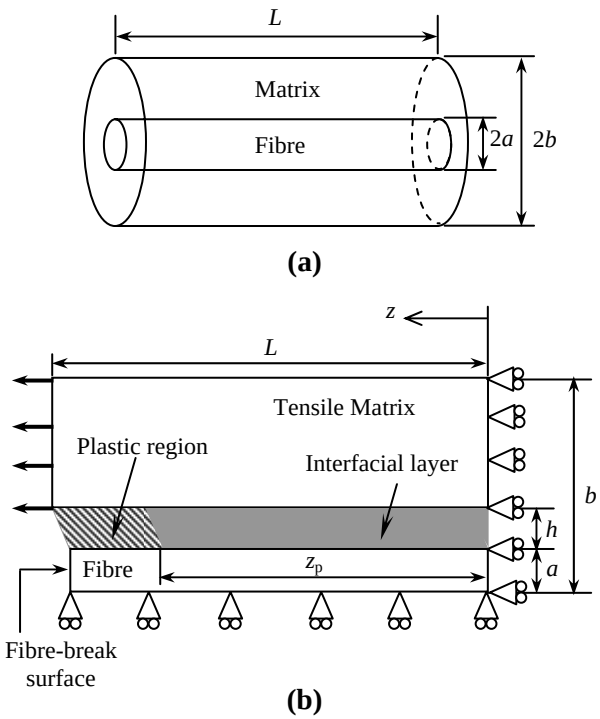

Fig.3. Schematic of the present model and definition of parameters: (a) cylindrical model, (b) idealized model composite with the matrix divided into tensile and shear parts

Assuming that the axial strain localization of the tensile matrix is negligible, the axial displacement of the tensile matrix, u_c, is written as

$$u_c = \varepsilon_c z \tag{1}$$

where ε_c is logarithmic strain of the composite. The shear strain rate in the plastic region, $\dot{\gamma}$, is given by J_2 flow theory and elasticity as follows:

$$\dot{\gamma} = \frac{\dot{\tau}}{G_m} + 2\lambda\tau \tag{2}$$

where λ is a proportionality factor enforcing normality of plastic strains to the yield surface, and the superposed dot represents differentiation with respect to time. Since an equivalent stress is written as $\sqrt{3}\tau$ in the interfacial layer, Eq. 2 is rewritten as

$$\dot{\gamma} = \frac{1}{A}\dot{\tau} \tag{3}$$

The coefficient A is a function of the elastic and plastic properties of the constituents and given as follows:

$$A=\left[\frac{1}{G_{\mathrm{m}}}+\alpha\frac{3\left(E_{\mathrm{m}}-E_{\mathrm{m}}^{\mathrm{p}}\right)}{E_{\mathrm{m}}E_{\mathrm{m}}^{\mathrm{p}}}\right]^{-1} \tag{4}$$

where $E_{\mathrm{m}}^{\mathrm{p}}$ is plastic tangent modulus of the matrix and

$$\alpha=\begin{cases}0 & \text{(elastic or unloading)}\\ 1 & \text{(plastic and loading)}\end{cases}$$

Using equilibrium of forces acting on the fibre, the interfacial shear stress, τ, is related to the fibre axial displacement, u, as

$$\tau=-\frac{a}{2}\cdot E_{\mathrm{f}}\cdot\frac{\partial^2 u}{\partial z^2} \tag{5}$$

where E is Young's modulus. The subscript f refers to fibre. Since the interfacial shear strain is assumed to be constant against the fibre radial direction in the interfacial layer, the shear strain is approximated as follows:

$$\gamma=\left(u_{\mathrm{c}}-u\right)/h \tag{6}$$

Combining the equations above, the following differential equation with respect to $\dot{u}$ is obtained and given by

$$\frac{\partial^2\dot{u}}{\partial z^2}-\frac{2A}{ahE_{\mathrm{f}}}\cdot\dot{u}=-\frac{2A}{ahE_{\mathrm{f}}}\dot{\varepsilon}_{\mathrm{c}}\cdot z \tag{7}$$

Eq.7 is the governing equation to be solved. Then, boundary conditions are needed to solve Eq.7. At the fibre-break point, the fibre axial stress is zero, and the fibre axial strain is equal to the applied strain of composite far from the fibre break. These boundary conditions are as follows:

$$E_{\mathrm{f}}\left.\frac{\partial u}{\partial z}\right|_{z=L}=0 \tag{8}$$

$$\left.\frac{\partial u}{\partial z}\right|_{z=0}=\varepsilon_{\mathrm{c}} \tag{9}$$

Eq.7 is solved by a finite difference scheme in the following section.

2.2 Finite Difference Scheme

Finite difference scheme is used to solve Eq.7. The fibre is discretized into N equal segments of length $\Delta z=L/N$. In the present model, L is taken to be sufficiently long such that the solutions represent an infinite fibre. The time history of the loading is divided into two segments. The first segment is when the fibre just breaks, and the second time segment is the following cyclic loading. During the first segment, the traction at the broken end of the fibre is released gradually to zero, and the rate of the applied strain is zero. Therefore, the boundary condition at the fibre-break point becomes as follows:

$$E_{\mathrm{f}}\left.\frac{\partial u}{\partial z}\right|_{z=L}=E_{\mathrm{f}}\left(\varepsilon_{\mathrm{fr}}-\varepsilon_{\mathrm{b}}\right) \tag{10}$$

where $\varepsilon_{\mathrm{fr}}$ is the strain at which a fibre break occurs and ε_{b} is sum of the released strain at the broken end of the fibre until time step t. During the second segment, the applied strain rate is not zero, but the traction at the broken end of the fibre is zero ($\varepsilon_{\mathrm{b}}=\varepsilon_{\mathrm{fr}}$). Both of these time segments are discretized into a finite number of time steps Δt. Using centered finite difference scheme, Eq. 7 is rewritten by the increment of the nodal displacements $\Delta u_{\mathrm{i}}^{t+1}$ and given by

$$\Delta u_{i+1}^{t+1}-\left(2+\frac{2A}{ahE_{\mathrm{f}}}\Delta z^2\right)\cdot\Delta u_i^{t+1}+\Delta u_{i-1}^{t+1}=-\frac{2A}{ahE_{\mathrm{f}}}\Delta\varepsilon_{\mathrm{c}}\cdot z_i \tag{11}$$

where $\Delta\varepsilon_{\mathrm{c}}$ is equal to $\dot{\varepsilon}_{\mathrm{c}}\Delta t$. i denotes positions along the fibre in z-direction: i=1 at z=0 (far from fibre-break point) and i=N at z=L (fibre-break point). The increments of fibre axial displacements calculated from Eq.11 are used to calculate increments of the interfacial shear and fibre axial stresses.

In the case of cyclic loading, since not only the plastic deformation under loading but also the reverse plastic deformation under unloading can occur as indicated in Fig.4, we conduct the calculation as follows; denoting the boundary node number between the elastic and plastic regions as *ia* and the number between the plastic and reverse plastic regions as *ib*, we define two parameters, r_{a} and r_{b}, as

$$r_{\mathrm{a}}=\frac{\tau_{\mathrm{Y}}-\tau_{ia\text{-}1}^{t}}{\Delta\tau_{ia\text{-}1}^{t+1}},\quad r_{\mathrm{b}}=-\frac{\tau_{\text{-}\mathrm{Y}}-\tau_{ib\text{-}1}^{t}}{\Delta\tau_{ib\text{-}1}^{t+1}} \tag{12}$$

where τ_{Y} is shear yielding stress of the matrix and equal to $\sigma_{\mathrm{Y}}/\sqrt{3}$ and $\tau_{\text{-}\mathrm{Y}}$ is $-\tau_{\mathrm{Y}}$. Not to violate the

yielding condition, the increment of the applied strain, $\Delta\varepsilon_c$, and the increments of the stresses, $\Delta\sigma_f$ and $\Delta\tau$, calculated at time step t+1 are modified to the exact increments by multiplying r_a under loading and r_b under unloading in the case of $0<r_a,r_b<1$. If this modification of the increments is not conducted, the calculations will result in misleading of the stress states. Flowchart of the present analysis is presented in Fig.5.

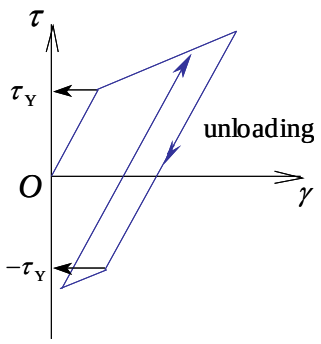

Fig.4. Schematic of shear stress-strain relationship in shear layer under cyclic loading

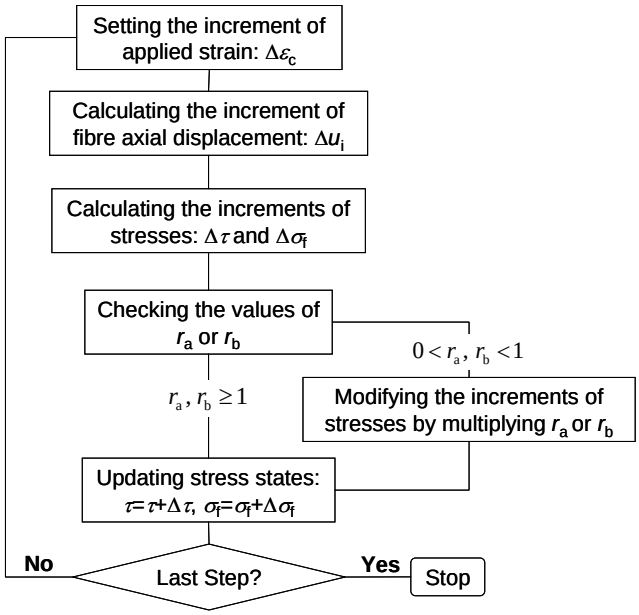

Fig.5. Flowchart of the present analysis

2.3 Stress Distribution

We calculated the stress states under cyclic loading between ε_c =0.02 and ε_c =0. We used a model proposed by Okabe and Takeda [2] as the model employing the total strain theory. Mechanical properties of the constituents used in the calculation are listed in Table1. In this calculation, the matrix does not yield in tension since yielding strain of the matrix is obtained as 0.02 from Table1. Fig.6 presents distributions of the fibre axial and interfacial shear stresses derived from the two different analyses.

Table 1. Mechanical properties of the constituents used in the calculations

	Fibre	Matrix
E (GPa)	78.0	3.0-
E^p (GPa)	-	0.10
Poisson's ratio ν	0.20	0.40
Diameter (mm)	0.012	0.50
σ_Y (MPa)	-	60.0

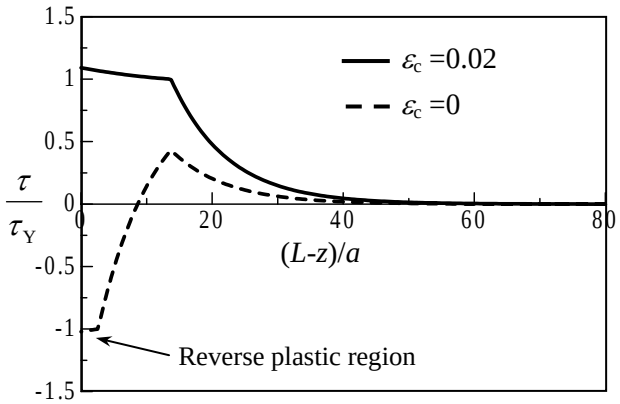

(a)

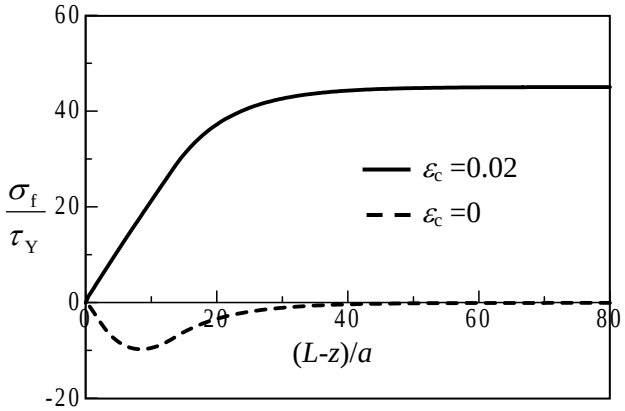

(b)

Fig.6. Distributions of interfacial shear and fiber axial stresses against distance from fibre-break point under cyclic loading between ε_c =0.02 and ε_c =0 obtained from the present model and the deformation theory model [2]: (a) interfacial shear stress (b) fibre axial stress

As a natural result, both shear and fibre axial stresses derived from the deformation theory model are identical with the results of the present model at ε_c =0.02 and equal to zero at ε_c =0. According to Fig.6, it is confirmed that the present model can consider an effect of the difference of the strain path since the stress distributions at $\varepsilon_c = 0$ are different from the distributions before loading, i.e. $\sigma_f = 0$ and $\tau = 0$. From this point of view, we can know that the stress states derived from the present model dramatically vary along with the difference of the strain path. In addition to that, Fig.6 indicates that the reverse plastic deformation occurs in the vicinity of the fiber-break point. Moreover, the fibre axial stress becomes compressive near the fibre break under unloading. These results are interesting since both the plastic deformation of the matrix and the compressive stress in the fibre occur even if overall behavior of the composite is elastic and not compressive.

3 Finite-element Analysis

Finite-element calculations were conducted to assess the validity of the stress distributions derived from the present analysis. The model is illustrated in Fig.3b. The commercial finite-element package Marc was used. The length of the model, *L*, is chosen such that the interfacial shear stress is approximately zero at $z = 2L/3$ [4]. The model is divided into 11,616 numbers of elements. The model is extended incrementally untill the applied strain reaches to the maximum value, and then the applied strain is removed incrementally to the minimum value. The results for the fibre axial and interfacial shear stresses are compared with the present shear-lag model.

Fig.7 shows distributions of the interfacial shear and fibre axial stresses at $\varepsilon_c = 0.02$ and at $\varepsilon_c = 0$ unloaded from $\varepsilon_c = 0.02$. According to Fig.7, the present shear-lag results are shown to be in good agreement with the FEM results. Therefore, it is confirmed that the present shear-lag analysis can appropriately give a valid stress states under cyclic loading even though it is distinctly simpler than the FEM analysis. In addition, the shear-lag analysis does not require such a great amount of time for calculation as FEM due to its simplification. Hence, we can know that the present shear-lag analysis can properly predict the stress states in and around the broken fibre under cyclic loading with much advantage in calculation time.

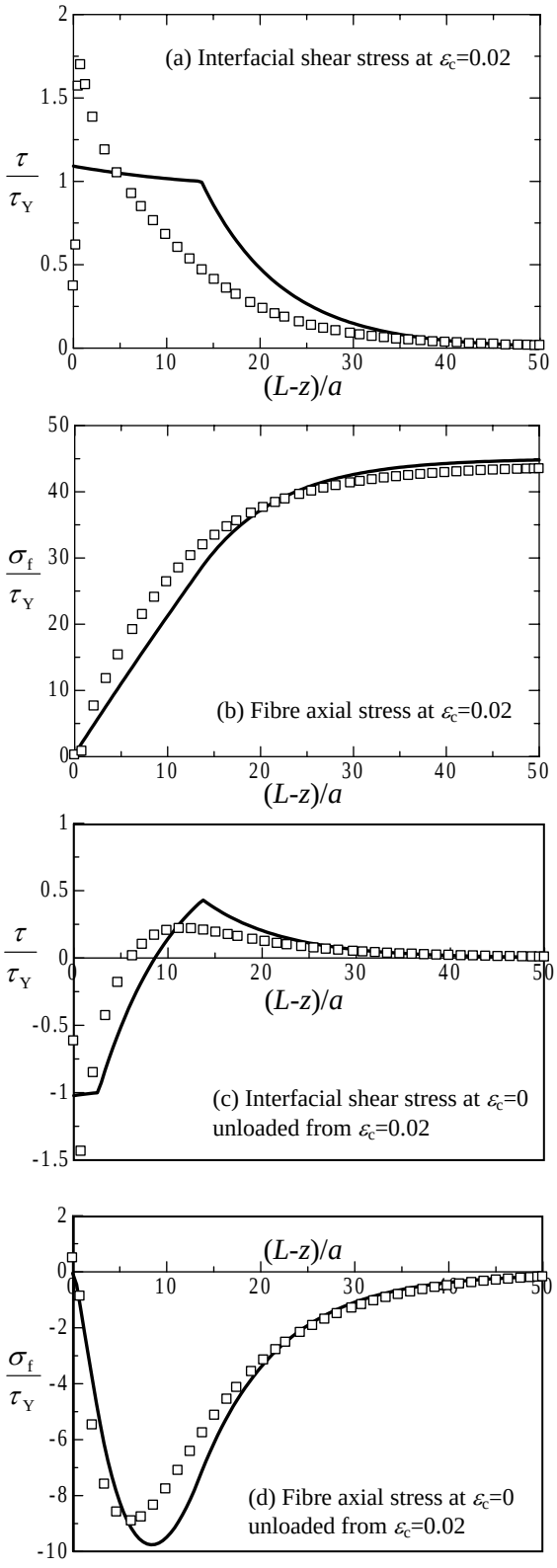

Fig.7. Comparison of the present shear-lag analysis (solid lines) and FEM (discrete points). The stress distributions are plotted as a function of distance from fibre break at $\varepsilon_c = 0.02$ and $\varepsilon_c = 0$ unloaded from $\varepsilon_c = 0.02$.

4 Discussions

Fig.8 shows variation of the plastic shear strain at the interface, $\Delta\gamma_p$, against distance from the fibre-break point under the different cyclic loading.

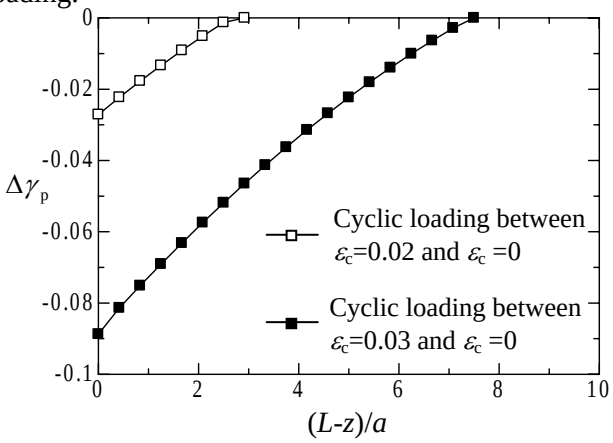

Fig.8. Relationship between plastic shear strain range and distance from fibre-break point under two different cyclic loading

From Fig.8, we can know that $\Delta\gamma_p$ increases along with an increase of the maximum value of the applied strain, and $\Delta\gamma_p$ is equal to zero under the cyclic loading between $\varepsilon_c = 0.01$ and $\varepsilon_c = 0$. Besides, the region in which changing of the plastic shear strain occurs is identical to the reverse plastic region.

Considering the fatigue equations of Coffin-Manson type, interfacial debonding can occur in the vicinity of the fibre-break point by cyclic loading; in other words, the debonding will not initiate under the specific loading condition in which the reverse plastic region does not occur, such as the cyclic loading between $\varepsilon_c = 0.01$ and $\varepsilon_c = 0$. Therefore, combination of the present model and the fatigue equations will enable us to predict initiation of the interfacial debonding by low cycle fatigue. In addition, experimental observation of the fiber-matrix interface during SFC test under cyclic loading will be effective to prove the validity of the present model.

5 Concluding Remarks

In this paper, an elasto-plastic shear-lag analysis was developed to predict the stress distribution in and around a broken fibre under cyclic loading. J_2 flow theory was employed as a constitutive equation of the matrix, and an incremental analysis was conducted. The present analysis turned out to be able to take an effect of the difference of the strain path into consideration. Moreover, the stress states obtained from the present model were significantly different from the results derived from the model applying the deformation theory. Comparison of the stress distributions with the FEM result was also conducted, and it was confirmed that the present model can appropriately predict the stress distributions in and around the broken fibre under cyclic loading.

Acknowledgement

Part of this study has been carried out with financial support from Mizuho Foundation for the Promotion of Sciences and 21st Century COE Program in Waseda University.

References

[1] Kelly A. and Tyson W.R. “Tensile properties of fibre reinforced metals: copper-tungsten and copper-molybdenum”. *Journal of Mechanics and Physics of Solids*, Vol. 13, pp.329-350, 1965.

[2] Okabe T. and Takeda N. “Elastoplastic shear-lag analysis of single-fiber composites and strength prediction of unidirectional multi-fiber composites”. *Composites: Part A: applied science and manufacturing*, Vol. 33, pp.1327-1335, 2002.

[3] Kimura S., Koyanagi J., Hama T. and Kawada H. “Evaluation of the interfacial properties in polymer matrix composite: experiments and elasto-plastic shear-lag analysis”. *Key Engineering Materials*, Vols. 340-341, pp.167-172, 2007.

[4] Landis C.H. and McMeeking R.M. “A shear-lag model for a broken fiber embedded in a composite with a ductile matrix”. *Composites Science and Technology*, Vol. 59, pp. 447-457, 1999.

[5] Kimura S., Koyanagi J., Hama T. and Kawada H. “An improved shear-lag model for a single fiber composite with a ductile matrix”. *Key Engineering Materials*, Vols. 334-335, pp.333-336, 2007.

[6] Budiansky B., Hutchinson J.W. and Evans A. “Matrix fracture in fiber-reinforced ceramics”. *Journal of the Mechanics and Physics of Solids*, Vol. 34, No.2, pp.167-189, 1986.

Appendix A. Thickness of Interfacial Layer

In this appendix, the thickness of the interfacial layer, *h* is derived as a function of radii of the fibre and matrix, *a* and *b*. The shear stress is assumed to be constant against the fibre radial direction in the present model, however in detail the shear stress is distributed along with the distance from the fibre-matrix interface, *r*, and given as

$$\tau = \frac{k\left(b^2 - r^2\right)}{ar}\tau_{\mathrm{i}} \qquad \text{(A1)}$$

where τ_{i} is interfacial shear stress. k is given as

$$k = \frac{a^2}{b^2 - a^2} \qquad \text{(A2)}$$

Then, the value of h is obtained from the correspondence of the shear strain energy contribution between the simplified present model and the detailed model [6], i.e.

$$\frac{\pi \cdot h(2a+h)}{2G_{\mathrm{m}}}\int_0^L \tau_{\mathrm{i}}^2 dz = \frac{1}{2G_{\mathrm{m}}}\int_0^L\int_a^b \tau^2 2\pi r dr dz \qquad \text{(A3)}$$

Substituting Eq.A1 into Eq.A3, h is obtained as follows:

$$h = \left[\sqrt{2(1+k)^2 \cdot \ln\left(\frac{b}{a}\right) - \frac{1}{2} - k} - 1\right] \cdot a \qquad \text{(A4)}$$

Fig.A1 indicates the relationship between h/a and b/a. According to Fig.A1, the value of h is approximately equal to $2a$ when b is sufficiently large. Therefore, we use $h=2a$ in the present model.

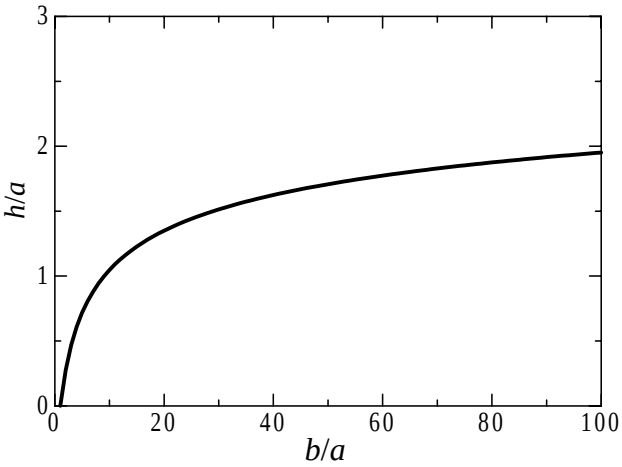

Fig.A1. Variation of normalized thickness of interfacial layer against normalized radius of matrix obtained from Eq.A4